Environ. Sci. Technol. **2010,** *44,* 7878–7883

Fabrication of a Novel Atrazine Biosensor and Its Subpart-per-Trillion Levels Sensitive Performance

ZHIMIN YU, GUOHUA ZHAO,* MEICHUAN LIU, YANZHU LEI, AND MINGFANG LI

Department of Chemistry, Tongji University, 1239 Siping Road, 200092 Shanghai, China

Received May 10, 2010. Revised manuscript received September 3, 2010. Accepted September 5, 2010.

The present study describes an atrazine biosensor with the detection limit of 0.1 part-per-trillion (ppt). The atrazine biosensor is fabricated on tyrosinase-immobilized vertical growth TiO_2 nanotubes (Tyr/TiO_2−NTs), based on the inhibition of tyrosinase by atrazine. The designed Tyr/TiO_2−NTs present excellent applicability in atrazine determination, with high sensitivity and stability, and rapid response. The outstanding sensing characteristics for atrazine is attributed to the appropriate bioelectrochemical interface of Tyr/TiO_2−NTs, resulting from the preponderant tubular structure, excellent biocompatibility, and hydrophilicity of TiO_2−NTs. The atrazine biosensor possesses a wide detection range from 0.2 ppt to 2 part-per-billion (ppb). The practical application of the biosensor is realized for the determination of atrazine and the analysis of its transport in soil samples. A new method for determination of atrazine in soil samples is thus established, which greatly simplifies the preparation procedure of sample and is helpful to evaluate the pollution risk of atrazine to soil, groundwater, and surface water.

Introduction

Atrazine (2-chloro-4-ethylamino-6-isopropylamino-1,3,5-triazine), because of its high efficiency and other features, has become one of the most widely used herbicides (*1*−*3*). It is a putative endocrine disruptor (*4, 5*) and may cause serious health risks even at very low levels (ppb) (*6*). The long-term exposure of creatures to atrazine with low concentration may induce subacute injury and potential hazards to the body. Although studies on the toxicity of atrazine on human have not been completely conclusive, atrazine exposure in rodent models has identified reproductive and developmental abnormalities (*7*−*10*). The maximum level for atrazine contamination is 3.0 ppb in drinking water, as established by the US Environmental Protection Agency. Thus it is of great significance to accurately quantify the compound at low concentrations.

Many well-established analytical methods are based on chromatographic determination, such as gas chromatography (*11*), high-performance liquid chromatography (*12*), and gas chromatography−mass spectrometry (*13*), which have been widely used for the detection of atrazine at trace levels. However, these methods are complex, time-consuming, and costly, especially requiring an exhaustive step for sample preparation, with bulky instruments. Due to the advantages such as simplicity, sensitivity, operational feasibility in turbid media, and easy miniaturization, electrochemical sensors have been considered for detecting atrazine. One of the major drawbacks to the electroanalytical technique is the use of mercury electrode at the detection limit of ppb (*14, 15*), because atrazine is only electroactive on mercury surface, which presents hazardous effects. In order to avoid the mercury contamination, several alternative electrodes have been proposed, and modified electrochemical biosensors have attracted extensive attention. Touloupakis et al. (*16*) immobilized photosynthetic thylakoid, the mutant resistant to atrazine, on the surface of screen-printed sensors with a detection limit of 2.15 ppb for atrazine. Biotinylated anti-triazine Fab fragment was attached to the PPy/neutravidin modified electrode to detect atrazine in the range of 0.1−200 ppb (*17*). A tyrosinase-immobilized biosensor may also be used for the detection of atrazine, based on that atrazine inhibits the catalytic activity of tyrosinase to some substrates, such as phenols (*18, 19*). However, because enzymes are highly unstable and the intermediate radicals formed may inactivate the enzyme and foul the electrode surface, the sensitivity is not satisfactory. For this reason, it has been the focused subject to improve the sensitivity and stability of biosensors (*20*).

In this work, to fabricate an atrazine biosensor with high stability and sensitivity, tyrosinase is immobilized on the surface of vertical growth TiO_2−NTs. It is realized that the sensitivity can be improved remarkably by constructing appropriate bioelectrochemical interface, which also improves the stability of tyrosinase, the load of biomolecules, and the electron transfer. It is well-known that such TiO_2−NTs possess excellent characteristics in applications for biomaterials. Biomolecules can retain their bioactivities and present high stability on the surface of TiO_2−NTs due to the excellent biocompatibility and high hydrophilicity (*21, 22*). Most importantly, abundant biomolecules may be immobilized because of the highly ordered vertically aligned TiO_2−NTs with large surface area, which can provide much more space for enzyme adsorption and confine biomolecules in the inner nanospaces (*23*). These characteristics will lead to excellent biosensors with high stability and sensitivity.

The biosensor fabricated in this work is for detecting atrazine in soil. Due to the large amount of atrazine used per unit area (the recommended application amount of atrazine by the agricultural sector: 1.7−2.8 kg ha^{-1}) and continuous use for many years, serious environmental problems have become apparent (*24*−*26*). The half-life of atrazine is more than 200 days, so it can easily accumulate in the soil and transport to the deep soil by the rain and irrigation water (*27, 28*). Therefore, the determination of atrazine in soil is of great environmental significance. A novel portable atrazine electrochemical biosensor with rapid response, high stability, and sensitivity is prepared in this work. This biosensor is used to detect atrazine and analyze its transport in soil, which is helpful to evaluate its pollution risk to surface water and groundwater.

Experimental Section

Reagents and Apparatus. Tyrosinase (5730 U/mg) and atrazine (purity >97%) were purchased from Sigma. Pure titanium foils (99.9% purity) were used for anodic oxidation. All the other reagents were of analytical grade and used

* Corresponding author phone: +86-21-65981180; fax: +86-21-65982287; e-mail: g.zhao@tongji.edu.cn.

10.1021/es101573s
Published on Web 09/20/2010

SCHEME 1. Schematic Illustration for Mechanism of the Biosensor

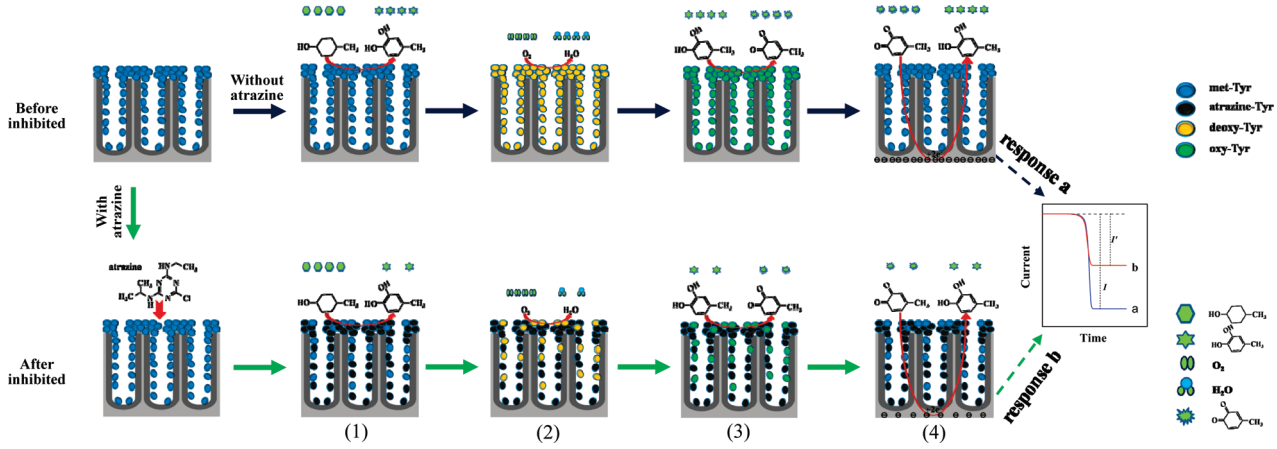

without further purification. Double-distilled water was used throughout the experiments.

Field emission scanning electron microscope (EFEG-SEM) and X-ray diffraction (XRD) were used to characterize the morphology and crystal structure of the as-prepared electrodes. High-performance liquid chromatography (HPLC, 1100, Agilent) was used to detect the atrazine as reference method.

Design and Construction of Biosensor. Highly ordered and vertically aligned TiO_2−NTs were primarily fabricated on Ti substrate by anodic oxidation (optimized in the Supporting Information (S1 of SI)). Before immobilizing tyrosinase, the electrode was first electrochemically pretreated at a constant potential of −1.5 V in neutral 2 M NH_4Cl aqueous electrolytes for 3 s. After having been rinsed by distilled water and dried, the surface of the pretreated TiO_2−NTs electrode (5 mm^2; diameter 2.5 mm) was covered with 20 μL of 50 U μL^{-1} tyrosinase solution and 5 μL of 2.5% glutaraldehyde aqueous solution by dropping with a microsyringe. After reaction for 10 min, the glutaraldehyde cross-linked the enzyme molecules, and then the electrode was dried immediately under a constant flux of N_2. After having been rinsed by distilled water and dried, the acquired tyrosinase-immobilized TiO_2−NTs (Tyr/TiO_2−NTs) electrode was stored at 4 °C in a refrigerator when not used.

Bioelectrochemistry Experiment. All the electrochemical measurements were performed using a conventional three-electrode cell system and a CHI 660c electrochemical workstation. TiO_2−NTs or Tyr/TiO_2−NTs electrode was employed as the working electrode, while a saturated calomel electrode (SCE) and a platinum electrode served as the reference and counter electrode, respectively. Buffers were purged with high-purity oxygen for at least 10 min before experiments, and an oxygen environment was kept over solutions in the cell to preserve the oxygen solution. All experiments were performed at room temperature.

Cyclic voltammetry (CV) was used to study the response of the TiO_2−NTs and Tyr/TiO_2−NTs electrode toward *p*-cresol, and amperometric measurements with Tyr/TiO_2−NTs electrode were performed to optimize experimental variables and with atrazine biosensor to determinate atrazine.

Results and Discussion

High-Sensitivity Performance of the Atrazine Biosensor. The detection of environmental pollutants by enzyme-immobilized biosensor is mainly based on the mechanism that the pollutants inhibit the biological activity of the enzyme to substrates. In detecting atrazine with this tyrosinase-immobilized biosensor, the percentage inhibition (Δi%) of biosensor response was recorded as a function of atrazine concentration

$$\Delta i(\%) = \frac{I - I'}{I} \times 100$$

where I is the biosensor response to the substrate in the absence of pesticide, and I' is the biosensor response after being "incubated" in the presence of atrazine (Scheme 1).

According to the mechanism, the sensitivity of the atrazine biosensor to substrate is a key factor of its sensitivity to atrazine and was thus investigated. The electrochemical features of the Tyr/TiO_2−NTs were first evaluated by CV. Figure 1A depicts the CV of Tyr/TiO_2−NTs in 0.1 M PBS (pH 7.0) without and with 0.1 mM *p*-cresol. Only background current is observed in the blank PBS (curve a), while the CV changes dramatically with an obvious increase of the reduction current when *p*-cresol is added (curve b). The comparison on TiO_2−NTs electrode without immobilized tyrosinase is made with CV. Under the same circumstance, no reduction signal is observed in the presence of *p*-cresol on the TiO_2−NTs (inset of Figure 1A). Obviously, the reduction peak on Tyr/TiO_2−NTs (curve b) is attributed to the reduction of quinone liberated from the enzyme reaction catalyzed by tyrosinase on the electrode surface.

A typical current−time plot for the Tyr/TiO_2−NTs on the successive step addition of *p*-cresol is obtained in 0.1 M PBS (pH 7.0) at the applied potential of −500 mV (S2 of the SI). As shown in Figure 1B, the Tyr/TiO_2−NTs exhibit a rapid response to the change of substrate concentration and reach steady-state current within 5 s. The reduction current at the electrode is proportional to the concentration of *p*-cresol in the range from 5×10^{-7} to 1.55×10^{-4} M according to the calibration curve (inset of Figure 1B). Thus the Tyr/TiO_2−NTs can be used in a wide range of *p*-cresol, with a sensitivity toward *p*-cresol of 1900 mA M^{-1}, which is much higher than that on tyrosinase/gelatin modified GCE (20.1 mA M^{-1}) (*29*), titania sol−gel-derived tyrosinase-based amperometric biosensor (1300 mA M^{-1}) (*30*), and Tyr-MPA-AuE (33 mA M^{-1}) (*31*).

The apparent kinetic parameter of the Tyr/TiO_2−NTs, an indication of both the enzymatic affinity an d the enzyme−substrate kinetic constants, is estimated from the relationship of $1/I$ versus $1/C_{p\text{-cresol}}$. The apparent Michaelis−Menten constant (K_M^{app}) is determined from the electrochemical Lineweaver−Burk form of the Michaelis−Menten equation (*32*)

$$\frac{1}{I} = \frac{1}{I_{max}} + \frac{K_M^{app}}{C_{p\text{-cresol}} I_{max}} \quad (1)$$

where I is the steady state current after the addition of *p*-cresol, I_{max} is the maximum current under saturating substrate conditions, and $C_{p\text{-cresol}}$ is the *p*-cresol concentration in the solution. An electrochemical Lineweaver−Burk plot ($1/I$ versus $1/C_{p\text{-cresol}}$) leads to a straight line and provides values of K_M^{app}/I_{max} (slope) and $1/I_{max}$ (*y*-axis intercept). The K_M^{app} value displays the affinity of an enzyme for its substrate, and a lower K_M^{app} value indicates stronger substrate binding and higher catalytic activity. In the present study, K_M^{app} value is 24.7 μM for the enzyme immobilized (S3 of the SI), which is obviously lower than the reported values, such as 26.1 μM of the biosensor based on tyrosinase entrapped in a vapor deposited titania sol−gel membrane (*31*) and 721 μM of tyrosinase/gelatin modified GCE (*29*). The low K_M^{app} value obtained in this study indicates that the tyrosinase molecules doped into the bioelectrode configuration retain their bioactivity and have high affinity for *p*-cresol, consequently, allowing higher sensitivity. Thus the constructed Tyr/TiO_2−NTs is considered as an excellent biosensor.

The inhibition of atrazine to this biosensor was investigated. In the measurements, the atrazine biosensor was first immersed in the PBS and the signal was stabilized. Then 0.1 mM *p*-cresol solution (substrate) was added and I was measured. The atrazine biosensor was rinsed, and a new measurement was taken by dipping the refreshed biosensor

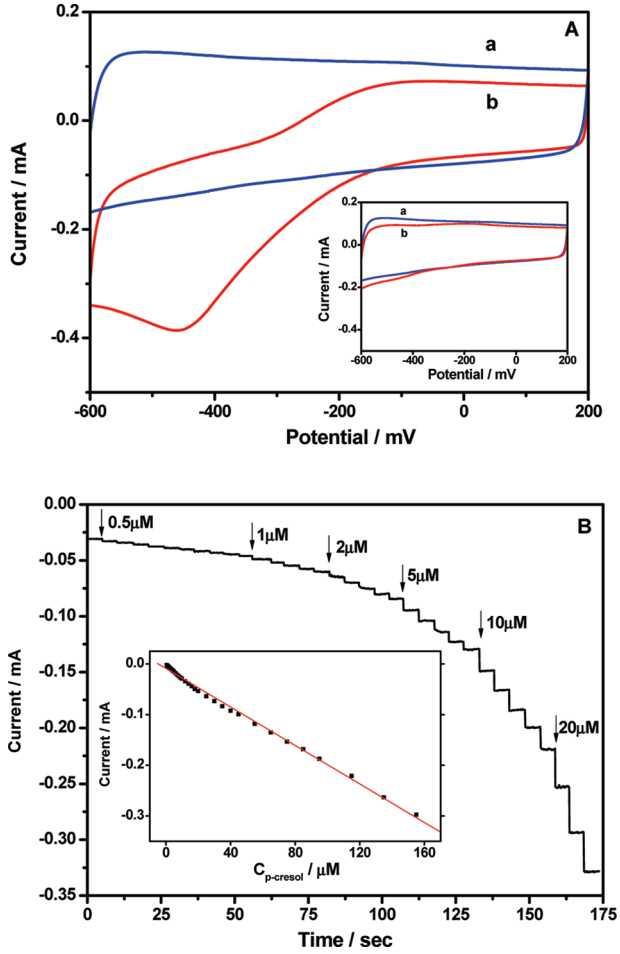

FIGURE 1. CVs of Tyr/TiO_2−NTs (A) and TiO_2−NTs (inset of A) in 0.1 M PBS without (a) and with 0.1 mM *p*-cresol (b); typical current−time curve (B) of Tyr/TiO_2−NTs with the addition of *p*-cresol in 0.1 M PBS at −500 mV and its calibration curves (inset of B).

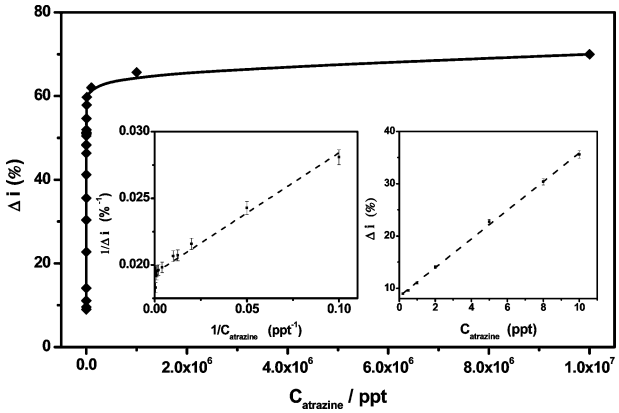

FIGURE 2. The inhibition curves of Tyr/TiO_2−NTs for atrazine in 0.1 M PBS (pH 7.0) at −500 mV inserts: calibration curves at low (A) and high concentrations of atrazine (B).

in atrazine-containing PBS solutions before adding 0.1 mM *p*-cresol and waiting for an incubation time of 10 min, while the enzyme and the inhibitor remained contact. After adding the *p*-cresol, I' was recorded and compared with the data obtained previously. After each inhibition measurement, the biosensor presented good operational stability and recoverability in 5 min by incubation in PBS containing the substrate (S4 of the SI).

The inhibition measurements were carried out in the range from 0.2 ppt to 10 ppm of atrazine concentration. Figure 2 (◆) shows that the inhibition percent (Δi(%)) increases with pesticide concentration, and the largest inhibition percent is more than 75%. Over the range from 10 ppt to 2 ppb, the relationship between $1/\Delta i$(%) and $1/C_{atrazine}$(ppt) is linear, with the regression equation of $1/\Delta i = 0.09029/C_{atrazine} + 0.01939$ and the correlation coefficient of 0.9871 (inset A of Figure 2). When the atrazine concentration is extremely low (0.2−10 ppt), the inhibition percent is lower than 35%, the relationship between Δi(%) and $C_{atrazine}$(ppt) is linear, and the regression equation is $\Delta i = 8.461 + 2.741 C_{atrazine}$ with the correlation coefficient of 0.9996 (inset B of Figure 2). When the inhibition percent is lower than 8%, the concentration of atrazine cannot be detected with this biosensor because of the signal-to-noise ratio, and the detection limit is calculated to be 0.1 ppt. Thus the detection range is from 0.2 ppt to 2 ppb. This low detection limit is much lower than that of Tyr-Au electrode (1.08 ppm) (*18*) and Tyr-PEDT-GC electrode (0.86 ppm) and even lower than that of the Tyr-AuNP-GC electrode (0.35 ppt) (*20*). Thus, a novel atrazine biosensor with excellent bioelectrochemical interface is successfully prepared, which presents high sensitivity and low detection limit.

We may explain the linearity from the enzyme kinetics as follows. Equation 1 determines the value of K_M^{app}, which presents the affinity of an enzyme for its substrate. The affinity of the enzyme for the inhibitor can be evaluated with inhibition constants K_I, which can be determined by using the following relationship (*32*)

$$K_M'^{app} = K_M^{app}\left(1 + \frac{C_{atrazine}}{K_I}\right) \quad (2)$$

where $K_M'^{app}$ is the apparent K_M^{app} of the immobilized enzyme in the presence of inhibitor, which can be determined by

$$\frac{1}{I'} = \frac{1}{I'_{max}} + \frac{K_M'^{app}}{C_{p\text{-cresol}} I_{max}} \quad (3)$$

In the competitive inhibition process, I'_{max} is equal to I_{max} (*32*). From eqs 1, 2, and 3, we have

$$\Delta i(\%) = \frac{I - I'}{I} \times 100 = \left(1 - \frac{C_{p-cresol} + K_M^{app}}{C_{p-cresol} + K_M^{app} + \frac{K_M^{app} C_{atrazine}}{K_I}}\right) \times 100 \quad (4)$$

where K_M^{app} and K_I are constants, so when $C_{p-cresol}$ is a certain value, eq 4 can be simplified as

$$\Delta i(\%) = p\frac{C_{atrazine}}{a + bC_{atrazine}} \quad (5)$$

where $a = C_{p-cresol} + K_M^{app}$, $b = (K_M^{app})/(K_I)$, and $p = 100(K_M^{app})/(K_I)$.

The inverse calculation on both sides of eq 5 gives

$$\frac{1}{\Delta i(\%)} = \frac{a}{pC} + \frac{b}{p} \quad (6)$$

Equation 6 illustrates the relation of $1/\Delta i(\%)$ and $1/C_{atrazine}$, which is the regression equation in the range of 10 ppt−2 ppb. When $C_{atrazine}$ is very small, the error will be quite large for eq 6. Moreover, when $C_{atrazine}$ is very small and $bC_{atrazine}$ is much less than a, $bC_{atrazine}$ can be neglected in the denominator of eq 5, so that eq 5 gives a linear relationship between $\Delta i(\%)$ and $C_{atrazine}$(ppt), corresponding to the low atrazine concentration from 0.2 to 10 ppt.

The detailed reasons for the high sensitivity and rapid response can be further exploited from the preponderant tubular structure, excellent biocompatibility, and hydrophilicity of TiO_2−NTs as well as the abundant immobilization of tyrosinase.

The structure and morphology of the TiO_2−NTs are first characterized by XRD and SEM. The XRD patterns (S5 of the SI) demonstrate that the TiO_2−NTs mainly consist of anatase phase ($2\theta = 25.2°$ and 54.2°), which corresponds to the (101) reflection of the crystalline anatase phase (JCPDS File 21-1272) and a rutile phase ($2\theta = 27.5$ and 36.1°), besides the major titanium crystal. According to the SEM characterization (S6 of the SI), the TiO_2−NTs are self-organized, vertically aligned, and compactly arranged with an average inner diameter of 80 ± 15 nm and the thickness of the tube wall of ca. 15 nm. This structure provides a large effective electrode surface for tyrosinase loading, which may facilitate the specific reaction between the substrate and the enzyme, resulting in a good amperometric response.

An adsorbed biomolecule may change its conformation to some extent because of biomolecule-surface interactions. Thus, the surface properties, especially the wettability of surfaces, will affect the adsorption and adhesion of biomolecules on the surfaces (*33*). The contact angle (CA) of water drop on the TiO_2−NTs (ca. 15°) (S7B of the SI) is smaller than that on Ti (ca. 55°) (S7A of the SI), reflecting its excellent hydrophilicity. Meanwhile, CAs of tyrosinase solution on Ti and TiO_2−NTs surface are also analyzed. The CA of tyrosinase on the TiO_2−NTs surface (ca. 10°) (S7D of the SI) is also smaller than that on Ti (ca. 55°) (S7C of the SI), indicating that the TiO_2−NTs interface is ideal for tyrosinase immobilization and can provide favorable microenvironment for maintaining its activity.

Electrochemical impedance spectroscopy (EIS) can provide the information of tyrosinase loading on the surface of TiO_2−NTs electrodes. The oxidation−reduction pair of $[Fe(CN)_6]^{3-}/[Fe(CN)_6]^{4-}$, in which the electron transfers fast and effectively, is widely used as electrochemical probe, especially applicable to characterize biomolecule-immobilized electrode. In this work, EIS measurements for different electrodes are performed in 0.1 M KCl solution containing 10 mM $[Fe(CN)_6]^{3-}/[Fe(CN)_6]^{4-}$ at the open circuit potential to assess their electrochemical properties. The electrochemical resistance of Tyr/TiO_2−NTs increases dramatically compared with that of TiO_2−NTs electrode (S8 of the SI), suggesting that tyrosinase is successfully immobilized on the surface of TiO_2−NTs. The reason for the resistance increase is that nonconductive proteins may obstruct electron transfer between the electrode and $[Fe(CN)_6]^{3-}/[Fe(CN)_6]^{4-}$. The surface coverage ratio (θ) of tyrosinase on the TiO_2−NTs can be estimated by using the equation $\theta = 1 - (R_{ct}^0/R_{ct})$ (*34, 35*), where R_{ct}^0 and R_{ct} are the resistances of the electrode before and after tyrosinase immobilization, respectively. For an optimized immobilization (S9 of the SI), the calculated θ of tyrosinase on TiO_2−NTs is 97%, indicating an almost saturated immobilization.

From the above results, the mechanism of the stable, rapid, and highly sensitive atrazine biosensor can be formulated. Tyrosinase is a bifunctional copper protein presenting at least two distinct binding sites, one of which has affinity for aromatic compounds (substrate site) (*36*). Before incubation: (1) large amount of tyrosinase loaded occupy the substrate sites and expedite the rate of enzyme catalytic reaction to *p*-cresol, producing a lot of 4-methylcatechol, while met-tyrosinase reduces to deoxy-tyrosinase. (2) With continuous oxygen flow and mixing, the reaction condition is always in oxygen saturation, resulting in a significant amount of active oxy-tyrosinase from the reaction of deoxy-tyrosinase and oxygen. (3) Abundant quinone is produced by the reaction of 4-methylcatechol and oxy-tyrosinase, while oxy-tyrosinase reverts to met-tyrosinase. (4) The enhanced current signal is attributed to the reduction of abundant quinone on the surface of the atrazine biosensor. 4-Methylcatechol is electrochemically regenerated avoiding intermediate polymer produced via direct electrochemical oxidation and resulting in a considerable amplification of the signal, which improves the sensitivity and stabilization of an enzymatic assay (*I*). After incubation, due to the reversible and competitive inhibition of atrazine, some of the substrate sites are deactivated, reducing enzyme catalysis, so the current signal decreases (*I'*). The detail enzyme catalytic reactions are as follows

$$p\text{-cresol} + \text{met-tyrosinase} \rightarrow \text{4-methylcatechol} + \text{deoxy-tyrosinase} \quad (1)$$

$$O_2 + \text{deoxy-tyrosinase} \rightarrow \text{oxy-tyrosinase} \quad (2)$$

$$\text{4-methylcatechol} + \text{oxy-tyrosinase} \rightarrow \text{2-methyl, 2-benzoquinone} + \text{met-tyrosinase} \quad (3)$$

$$\text{2-methyl-1, 2-benzoquinone} + 2e^- + 2H^+ \rightarrow \text{4-methylcatechol} \quad (4)$$

This mechanism has been described in Scheme 1.

The performance of the Tyr/TiO_2−NTs as an atrazine biosensor is further investigated for its pH range and temperature adaptability as well as the repeatability.

Broad pH applicability is of great significance in environmental control and monitoring. The pH value of the solution may have obvious effects on the bioactivity of tyrosinase. Thus the influence of pH on the amperometric response is investigated for 0.1 mM *p*-cresol in the pH range of 3.0−8.0 adjusted by PBS (0.1 M), as shown in Figure 3. The amperometric response changes slightly between pH 4.0 and 8.0, indicating that this atrazine biosensor can be used in a wide pH range.

Figure 3 also displays the amperometric response of the atrazine biosensor in the temperature range of 25 − 70 °C. The initial response of the electrode is obtained in the presence of 0.1 mM *p*-cresol at 25 °C. Then the electrode is immersed in the PBS (pH 7.0) for 1 h at a given temperature and the amperometric response is measured. The amperometric response changes slightly between 25−50 °C, dem-

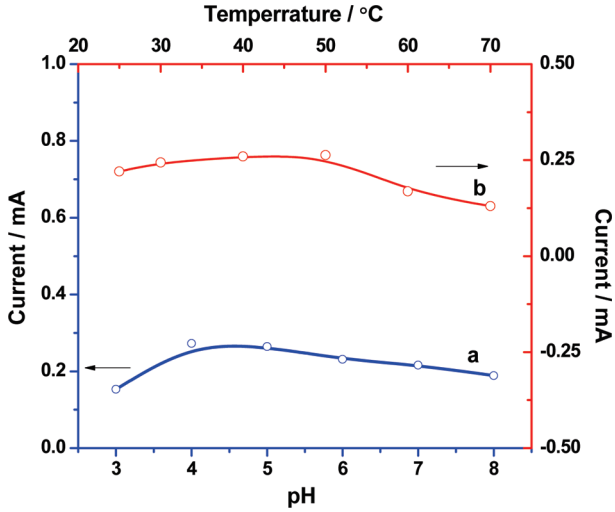

FIGURE 3. pH (a) and temperature (b) dependence of Tyr/TiO_2−NTs amperometric response to 0.1 mM *p*-cresol in 0.1 M PBS at an applied potential of −500 mV versus SCE.

onstrating that the TiO_2−NTs are good for maintaining the bioactivity of tyrosinase, so that the effective detection of atrazine can be realized in a wide temperature range.

Moreover, the repeatability of the atrazine biosensor is investigated by CV in 0.1 M PBS (pH 7.0) with 0.1 mM *p*-cresol. The mean steady-state peak current is 0.22 mA with a relative standard deviation of 4.2% for 20 continuous measurements. After the measurements, the atrazine biosensor is rinsed with double distilled water and stored at 4 °C. The investigation on long-term stability of the atrazine biosensor shows that it retains more than 90% of its initial activity after 4 weeks. The good stability of the atrazine biosensor may be mainly ascribed to the above-mentioned hydrophilicity interactions with TiO_2−NTs owing to their favorable wettability. Furthermore, the potential confining effects provided by the unique 3-D nanotubular structure of TiO_2−NTs may also stabilize the tyrosinase.

Detection of Atrazine in Soil Samples. The atrazine biosensor is used to detect atrazine in soil. The soil sample solution (S10 of the SI) is accurately diluted with PBS if the concentration of atrazine is out the linearity range. Figure 4 shows the spatial distribution of atrazine in soil. As a reference, the assayed samples are also studied with HPLC. The standard deviation of detecting results with the two methods is less than 5%, and the atrazine biosensor can detect atrazine in a lower concentration range. Most importantly, the preparation procedure of sample is greatly simplified by using the atrazine biosensor compared with HPLC, shortening the detection time and reducing possible errors caused by complex procedures. In addition, the standard addition method has been used to test the atrazine biosensor for more soil samples (S11 of the SI). In all cases the relative error is below 4% between the measured value and the assigned atrazine concentration at the level considered. On the other hand, since enzyme is a class of substances, the activity of tyrosinase may be affected by other inhibitors such as triazines, carbamates, and organophosphates. Thus the biosensor may be also affected by other inhibitors in practical applications.

Figure 4 shows that the concentration of atrazine reduces as the depth of soil increases. It is very high in the soil layer of 0−20 cm and reduces obviously in the layer of 20−30 cm, because a large amount of atrazine detains in the surface soil due to the adsorption. However, it is noteworthy that atrazine is still detected in the 60−70 cm depth, which may be due to the rapid downward migration of atrazine with preferential flow that reduce the soil filtration. This preferential transport induces large-scale pollution of deep soil and increases the difficulty of soil remediation. It is reported that atrazine can even transport to the soil layer deeper than 1 m to pollute the groundwater (*28*). In recent years, residual atrazine is measured in soil, groundwater, and surface water in many areas (*11*−*13*), which will reduce soil fertility and debase the quality of agricultural products, directly endangering human health. Thus, the detection of atrazine in soil will help us to understand the transport conditions of atrazine in the soil and will be valuable for the hazard assessment of groundwater and surface water.

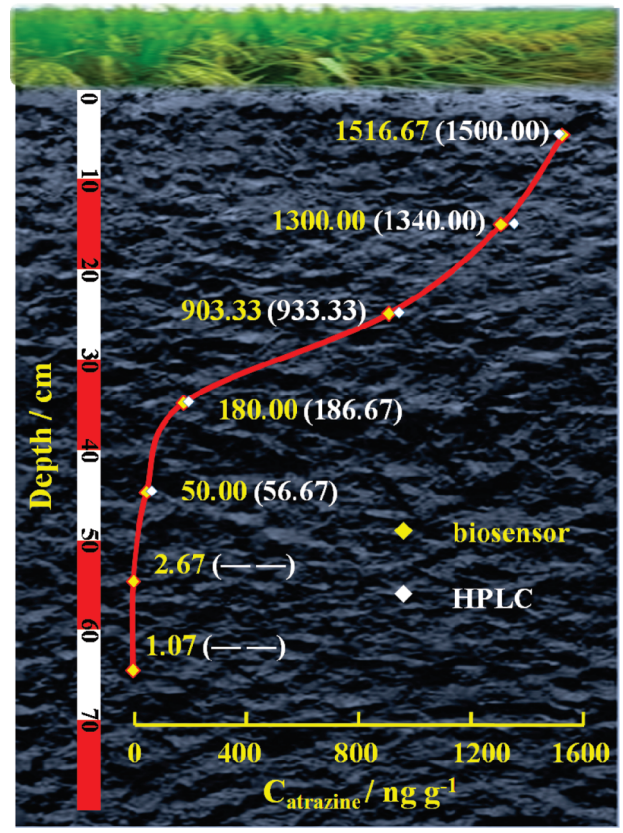

FIGURE 4. The spatial distribution of atrazine in soil.

Acknowledgments

This work was supported jointly by the National Natural Science Foundation of China (20877058 and 21077077), 863 Program (2008AA06Z329) from the Ministry of Science and Shanghai Educational Development Foundation (2007CG24). The authors would like to thank Professor Dongming Li for her help of technique writing.

Supporting Information Available

Preparation of TiO_2−NTs (S1), working potential (S2), Lineweaver−Burk plots for *p*-cresol (S3), the recoverability of the atrazine biosensor (S4), the XRD patterns of TiO_2−NTs (S5), SEM of TiO_2−NTs(S6), contact angles of water or tyrosinase solution drops on Ti and TiO_2−NTs surface (S7), EIS patterns of TiO_2−NTs, Tyr/TiO_2−NTs (S8), the effect of tyrosinase loading on the surface of the electrode (S9), the detailed experiment including preparation and testing of soil samples (S10), and the standard addition method (S11). The material is available free of charge via the Internet at http://pubs.acs.org.

Literature Cited

(1) Rohr, J. R.; Schotthoefer, A. M.; Raffel, T. R.; Carrick, H. J.; Halstead., N.; Hoverman., J. T.; Johnson, C. M.; Johnson, L. B.;

Lieske, C.; Piwoni, M. D.; Schoff, P. K.; Beasley, V. R. Agrochemicals increase trematode infections in a declining amphibian species. *Nature* **2008**, *455*, 1235–1239.
(2) Ma, W. T.; Cai, Z. W.; Jiang, G. B. Determination of atrazine, deethylatrazine and simazine in water at parts-per-trillion levels using solid-phase extraction and gas chromatography/ion trap mass spectrometry. *Rapid Commun. Mass Spectrom.* **2003**, *17*, 2707–2712.
(3) Buster, H. R. Atrazine and other s-trazine herbicides in lakes and rians in Switzerland. *Environ. Sci. Technol.* **1990**, *24*, 1049–1058.
(4) Chen, C.; Yang, S. G.; Guo, Y. P.; Gua, C. G.; Xu, B. Photolytic destruction of endocrine disruptor atrazine in aqueous solution under UV irradiation: Products and pathways. *J. Hazard. Mater.* **2009**, *172*, 675–684.
(5) Hayes, T. B. There is no denying this: Defusing the confusion about atrazine. *Bioscience* **2004**, *54*, 1138–1149.
(6) Kaur, J.; Singh, K. V.; Boro, R.; Thampi, K. R.; Raje, M.; Varshney, G. C.; Suri, C. R. Immunochromatographic Dipstick Assay Format Using Gold Nanoparticles Labeled Protein-Hapten Conjugate for the Detection of Atrazine. *Environ. Sci. Technol.* **2007**, *41*, 5028–5036.
(7) Stoker, T. E.; Guidici, D. L.; Laws, S. C.; Cooper, R. L. The effects of atrazine metabolites on puberty and thyroid function in the male Wistar rat. *Toxicol. Sci.* **2002**, *67*, 198–206.
(8) Rayner, J. R.; Enoch, R. R.; Fenton, S. E. Adverse effects of prenatal exposure to atrazine during a critical period of mammary gland growth. *Toxicol. Sci.* **2005**, *87*, 255–266.
(9) Ruiz, M. J.; Marzin, D. Genotoxicity of six pesticides by salmonella mutagenicity test and SOS chromstest. *Mutat. Res., Genet. Toxicol. Environ. Mutagen.* **1997**, *390*, 245–255.
(10) El-Sheekha, M. M.; Kotkatb, H. M.; Hammouda, O. H. E. Effect of atrazine herbicide on growth, photosynthesis, protein synthesis, and fatty acid composition in the unicellular green alga Chlorella Kessleri. *Ecotoxicol. Environ. Saf.* **1994**, *29*, 349–358.
(11) Tomkins, B. A.; Ilgner, R. H. Determination of atrazine and four organophosphorus pesticides in ground water using solid phase microextraction (SPME) followed by gas chromatography with selected-ion monitoring. *J. Chromatogr., A* **2002**, *972*, 183–194.
(12) Panuwet, P.; Nguyen, J. V.; Kuklenyik, P.; Udunka, S. O.; Needham, L. L.; Barr, D. B. Quantification of atrazine and its metabolites in urine by on-line solid-phase extraction-high-performance liquid chromatography-tandem mass spectrometry. *Anal. Bioanal. Chem.* **2008**, *391*, 1931–1939.
(13) Ma, W. T.; Jiang, G. B.; Cai, Z. W. Determination of atrazine and its deethylated degradation product in water and sediment by using gas chromatography/ion trap mass spectrometry. *Int. J. Environ. Anal. Chem.* **2005**, *85*, 1117–1125.
(14) Vaz, C. M. P.; Crestana, S.; Machado, S. A. S.; Mazo, L. H.; Avaca, L. A. Electroanalytical determination of the herbicide atrazine in natural waters. *Int. J. Environ. Anal. Chem.* **1996**, *62*, 65–76.
(15) dos, Santos, L. B. O.; Abate, G.; Masini, J. C. Developing a continuous flow-square wave voltammetry method for determination of atrazine in soil solutions using the hanging mercury drop electrode. *J. Braz. Chem. Soc.* **2006**, *17*, 36–42.
(16) Touloupakis, E.; Giannoudi, L.; Piletsky, S. A.; Guzzella, L.; Pozzoni, F.; Giardi, M. T. A multi-biosensor based on immobilized Photosystem II on screen-printed electrodes for the detection of herbicides in river water. *Biosens. Bioelectron.* **2005**, *20*, 1984–1992.
(17) Esseghaier, C.; Helali, S.; Ben, Fredj, H.; Tlili, A.; Abdelghani, A. Polypyrrole-neutravidin layer for impedimetric biosensor. *Sens. Actuators, B* **2008**, *131*, 584–589.
(18) McArdle, F. A.; Persaud, K. C. Development of an enzyme-based biosensor for atrazine detection. *Analyst* **1993**, *118*, 419–423.
(19) Besombes, J. L.; Cosnier, S.; Labbe, P.; Reverdy, G. A biosensor as warning device for the detection of cyanide, chlorophenols, atrazine and carbamate pesticides. *Anal. Chim. Acta* **1995**, *311*, 255–263.
(20) Kim, G. Y.; Shim, J.; Kang, M. S.; Moon, S. H. Optimized coverage of gold nanoparticles at tyrosinase electrode for measurement of a pesticide in various water samples. *J. Hazard. Mater.* **2008**, *156*, 141–147.
(21) Liu, M. C.; Zhao, G. H.; Zhao, K. J.; Tong, X. L.; Tang, Y. T. Direct electrochemistry of hemoglobin at vertically-aligned self-doping TiO_2 nanotubes: A mediator-free and biomolecule-substantive electrochemical interface. *Electrochem. Commun.* **2009**, *11*, 1397–1400.
(22) Zhao, G. H.; Lei, Y. Z.; Zhang, Y. G.; Li, H. X.; Liu, M. C. Growth and Favorable Bioelectrocatalysis of Multishaped Nanocrystal Au in Vertically Aligned TiO_2 Nanotubes for Hemoprotein. *J. Phys. Chem. C* **2008**, *112*, 14786–14795.
(23) Liu, M. C.; Zhao, G. H.; Tang, Y. T.; Yu, Z. M.; Lei, Y. Z.; Zhang, Y. N.; Li, D. M. A Simple, Stable and Picomole Level Lead Sensor Fabricated on DNA-based Carbon Hybridized TiO_2 Nanotube Arrays. *Environ. Sci. Technol.* **2010**, *44*, 4241–4246.
(24) Nicolai, D. J.; Stephan, K.; Diana, H.; Andreas, S.; Peter, B. Spatial Distribution and Characterization of Long-Term Aged 14C-Labeled Atrazine Residues in Soil. *J. Agric. Food Chem.* **2008**, *56*, 9548–9554.
(25) Graziano, N.; McGuire, M. J.; Roberson, A.; Adams, C.; Jiang, H.; Blute, N. 2004 National atrazine occurrence monitoring program using the Abraxis ELISA method. *Environ. Sci. Technol.* **2006**, *40*, 1163–1171.
(26) Tappe, W.; Groeneweg, J.; Jansch, B. Diffuse atrazine pollution in German aquifers. *Biodegradation* **2002**, *13*, 3–10.
(27) Silva, E.; Fialho, A. M.; Sa-Correia, I.; Burns, R. G.; Shaw, L. J. Combined bioaugmentation and biostimulation to cleanup soil contaminated with high concentrations of atrazine. *Environ. Sci. Technol.* **2004**, *38*, 632–637.
(28) Ma, W. T.; Fu, K. K.; Cai, Z. W.; Jiang, G. B. Gas chromatography/mass spectrometry applied for the analysis of triazine herbicides in environmental waters. *Chemosphere* **2003**, *52*, 1627–1632.
(29) Li, N.; Xue, M. H.; Yao, H.; Zhu, J. J. Reagentless biosensor for phenolic compounds based on tyrosinase entrapped within gelatine film. *Anal. Bioanal. Chem.* **2005**, *383*, 1127–1132.
(30) Kochana, J.; Gala, A.; Parczewski, A.; Adamski, J. Titania sol-gel-derived tyrosinase-based amperometric biosensor for determination of phenolic compounds in water samples. Examination of interference effects. *Anal. Bioanal. Chem.* **2008**, *391*, 1275–1281.
(31) Campuzano, S.; Serra, B.; Pedrero, M.; Villena, F. J. M.; Pingarron, J. M. Amperometric flow-injection determination of phenolic compounds at self-assembled monolayer-based tyrosinase biosensors. *Anal. Chim. Acta* **2003**, *494*, 187–197.
(32) de Albuquerque, Y. D. T.; Ferreira, L. F. Amperometric biosensing of carbamate and organophosphate pesticides utilizing screen-printed tyrosinase-modified electrodes. *Anal. Chim. Acta* **2007**, *596*, 210–221.
(33) Wu, S.; Ju, H. X.; Liu, Y. Conductive Mesocellular Silica-Carbon Nanocomposite Foams for Immobilization, Direct Electrochemistry, and Biosensing of Proteins. *Adv. Funct. Mater.* **2007**, *17*, 585–592.
(34) Song, Y. Y.; Li, Y.; Yang, C.; Xia, X. H. Surface electric field manipulation of the adsorption kinetics and biocatalytic properties of cytochrome c on a 3D macroporous Au electrode. *Anal. Bioanal. Chem.* **2008**, *390*, 333–341.
(35) Laviron, E. The use of linear potential sweep voltammetry and of ac voltammetry for the study of the surface electrochemical reaction of strongly adsorbed systems and of redox modified electrodes. *J. Electroanal. Chem.* **1979**, *100*, 263–270.
(36) Vidal, J. C.; Esteban, S.; Gil, J.; Castillo, J. R. A comparative study of immobilization methods of a tyrosinase enzyme on electrodes and their application to the detection of dichlorvos organophosphorus insecticide. *Talanta* **2006**, *68*, 791–799.

ES101573S